Measurement of the Muon Decay Spectrum with a Wire Spark-Chamber Spectrometer*†‡

DAVID FRYBERGER§
The Enrico Fermi Institute for Nuclear Studies and Department of Physics, The University of Chicago, Chicago, Illinois

(Received 16 June 1967)

The decay spectrum of the positive muon has been studied in a wire spark-chamber spectrometer of wide momentum acceptance. Both the parameters δ and ρ were determined. On the basis of 4.9×10^5 events, obtained in runs with different fields and targets, we find for the parameter governing the energy dependence of the asymmetry, the value $\delta=0.752\pm0.009$. From a spectrum of 1.7×10^6 events we find for the shape parameters of the isotropic spectrum $\rho=0.762\pm0.008$ (assuming $\eta\equiv0$), or $\eta=-0.7\pm0.5$ (assuming $\rho\equiv\frac{3}{4}$). These values for ρ and δ are in agreement with two-component neutrino theory. Using our value of δ and averages of the most accurate published values of the other muon decay parameters, we find that the scalar and tensor couplings (in charge retention ordering) can still account for as much as 30% of the interaction.

I. INTRODUCTION

IT has been shown[1–3] that the most general local (derivative-free, lepton-conserving) interaction Hamiltonian for polarized muon decay leads to the electron spectrum (with radiative corrections[4–6])

$$N(x,\mathbf{P}\cdot\hat{x})d^3x=[M(x;\rho,\eta)+(\mathbf{P}\cdot\hat{x})\xi B(x;\delta)]d^3x, \quad (1)$$

where x is the electron momentum in units of $m_\mu c/2$, $\mathbf{P}$ is the muon polarization, ρ and η are parameters governing the isotropic spectrum M, and δ and ξ (convenient parameters introduced by Kinoshita and Sirlin[3]) are parameters governing the asymmetric spectrum ξB. In addition to the four parameters ρ, η, ξ, and δ, there are two more which are not explicit in Eq. (1). These are the lifetime τ and helicity h, making a total of six observable decay parameters.

These decay parameters are bilinear functions of the ten (possibly complex) coupling constants which characterize the most general interaction Hamiltonian. Clearly, there are too few experimentally accessible quantities to determine the coupling constants unambiguously as long as one considers muon decay from a general point of view (i.e., as long as one does not postulate any *a priori* relationships to other weak interaction processes); the measured parameters can provide only consistency checks for given hypotheses. Jarlskog[7] has shown that if experiment yields the "$V-A$" values for ρ, δ, ξ, and h, then the Hamiltonian will be limited to a V and A interaction, but the A/V ratio (say, ϵ) and the degree of circular polarization of the neutrinos remain undetermined (see Appendix A); furthermore $\eta=0$ is implied automatically. On the other hand, if one postulates two-component neutrinos, then $\rho=\delta=\frac{3}{4}$ is implied while measurements of $h(=-\xi)$ and η will yield ϵ. (These relationships are illustrated in Fig. 8 which is discussed in Sec. VII.)

Notwithstanding the preceding cautionary remarks, it is obviously desirable to determine all the accessible parameters as accurately as possible. A program to do this is underway in this and other laboratories, and precision studies of the isotropic spectrum have already been published.[8,9]

The main aim of this paper is to discuss in detail[10] our experimental study of the asymmetric spectrum $\xi B(x)$ and its analysis in terms of the parameter δ. Among the decay parameters, δ is a particularly attractive one to determine because it is experimentally remarkably invulnerable to systematic effects (see Sec. VI, in particular Table V), and hence its accuracy is to a large extent determined by counting statistics alone.

A determination of δ is furthermore advantageous even from a purely statistical point of view. As is by now well known, the isotropic parameters ρ and η exhibit,[8] when determined from fits to a limited part (say, with $x>0.5$) of the isotropic spectrum, a considerable statistical correlation; i.e., one induces a large statistical uncertainty in the value of ρ by fitting simultaneously for η. Contrary to this situation, the two parameters of the asymmetric spectrum, i.e., δ and the product $P\xi$, are essentially uncorrelated statistically. Thus the full power of increased counting statistics can be used to improve the accuracy of δ.

* Research supported by the Office of Naval Research and NSF GP 6135 (Research).

† Thesis submitted to the Department of Physics, The University of Chicago, in partial fulfillment of the requirements for the Ph.D. degree.

‡ Fellow, Fannie and John Hertz Foundation, 1964–67.

§ Present address: Stanford Linear Accelerator Center, Stanford, California.

[1] C. Bouchiat and L. Michel, Phys. Rev. **106**, 170 (1957).

[2] S. Larsen, E. Lubkin, and M. Tausner, Phys. Rev. **107**, 856 (1957).

[3] T. Kinoshita and A. Sirlin, Phys. Rev. **107**, 593 (1957).

[4] S. M. Berman, Phys. Rev. **112**, 267 (1958).

[5] T. Kinoshita and A. Sirlin, Phys. Rev. **113**, 1652 (1959).

[6] V. P. Kuznetsov, Zh. Esperim. i Teor. Fiz. **37**, 1102 (1959) [English transl.: Soviet Phys.—JETP **37**, 784 (1960)].

[7] C. Jarlskog, Nucl. Phys. **75**, 659 (1966).

[8] B. A. Sherwood, Phys. Rev. **156**, 1475 (1967).

[9] M. Bardon, P. Norton, J. Peoples, A. M. Sachs, and J. Lee-Franzini, Phys. Rev. Letters **14**, 449 (1965); J. Peoples, Nevis Report No. 147, 1966 (unpublished).

[10] A preliminary analysis of this data has been published. R. D. Ehrlich, D. Fryberger, D. A. Jensen, C. Nissim-Sabat, B. A. Sherwood, and V. L. Telegdi, Phys. Rev. Letters **17**, 1118 (1966).

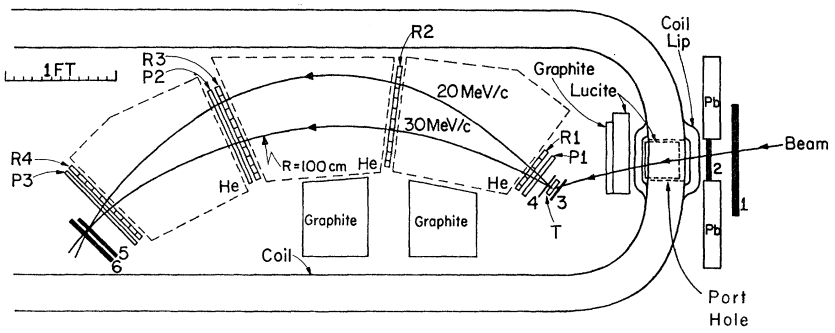

FIG. 1. Experimental arrangement. R1 through R4 and P1 through P3 are (parallel) wire spark chambers. The porthole produces at the target T a vertical field inhomogeneity of $<0.4\%$ which falls off rapidly. Spatial homogeneity of the field in the region of interest was such that $\sigma_B(\mathbf{x})/\bar{B}<0.1\%$ (including the perturbations of the porthole), temporal homogeneity (maintained by a feedback loop) such that $\sigma_B(t)/\bar{B}<0.03\%$.

Our primary objective was to determine δ with a standard deviation of less than 0.01. While determinations of δ are already available in the literature,[11,12] even the most precise of these ($\delta=0.782\pm0.031$) is not of an accuracy comparable to that of the most recent measurements[8,9] of the isotropic spectrum, which (assuming $\eta\equiv0$, as has become customary) determine ρ to better than 1%.

A second objective was a remeasurement of the isotropic spectrum. Such a study yields results of an accuracy roughly comparable to previous measurements[8,9] and gives us an improved understanding of the apparatus for this and future experiments. The agreement of these results with previous ones provides a worthwhile confirmation.

II. APPARATUS

Our measurement of the asymmetric spectrum is in essence a Garwin-Lederman experiment[13] in which the field of a wire spark-chamber spectrometer is used for both momentum analysis and precession. The experiment was performed using essentially the same spectrometer as is described in Refs. 8 and 14. The main changes were (1) the provision of a "porthole" in the magnet coils,[15] and (2) the use of a stops telescope (counters 3 and 4) instead of a single scintillator in which the π-μ-e chain was detected. The experimental setup (after provision of the porthole) is shown in Fig. 1. The scintillator dimensions are given in Table I.

The spark chambers and accessories (helium boxes, etc.) were mounted on a plate. Fiducial scribe lines, provided on the chambers, were used to ensure that the chambers were vertical. The spectrometer coordinate system was then established by measuring the locations of the scribe lines with a large milling machine. This procedure enables one to know the wire locations to ±0.003 in. The locations of the target and final counter 5, which were fastened to the magnet rather than to the spectrometer assembly, were determined by examining illumination plots (similar to those in Fig. 2) extracted from the data. As a check against "gross" errors, the relative positions of these external objects were verified by measurements using a precision scale (0.01-in. divisions); no disagreements were found.

Highly polarized ($P\sim70\%$) positive muons were injected into the magnet and stopped in a nondepolarizing target T (graphite or lithium). Graphite was selected initially as a compromise between stopping rate and energy loss. For better control of systematics, the graphite target was stepped. This stepped construction (see profile, Fig. 2) enabled us to collect spectra with different energy losses simultaneously. When the porthole was provided, the stop rate (per unit mass) increased and lithium was used.

The electronic logic is shown in Fig. 3. Each muon signature ($123\bar{4}$) opened two 5-μsec gates. The first gate was prompt and collected "real" events; the second was delayed by 17-μsec and collected "accidental" events. The opening of each gate started a timer (100-MHz digitron) which was provided with the conventional double-start/stop protection circuitry.[16] A trigger occurred when a positron signature $[(\bar{1}\bar{2}\bar{3})$

TABLE I. Scintillator dimensions.

Counter No.	Dimensions ($W\times H\times T$ in in.)
1	$8\times8\times\frac{1}{4}$
2	$5\times5\times\frac{1}{4}$
3 (C)[a]	$2\frac{5}{8}\times7\times\frac{1}{8}$
3 (Li)	$2\frac{5}{8}\times7\times\frac{1}{16}$
4 (C)[a]	$3\frac{1}{8}\times7\times\frac{1}{16}$
4 (Li)	$3\frac{1}{8}\times7\times\frac{1}{32}$
5	$6\times6\times\frac{1}{4}$
6	$9\times9\times\frac{3}{8}$

[a] Counters 3 and 4 differed for the C and Li data.

[11] R. J. Plano, Phys. Rev. **119**, 1400 (1960).
[12] H. Kruger, University of California Radiation Laboratory Report No. UCRL-9322, 1961 (unpublished). We wish to thank R. D. Sard for bringing this unpublished work to our attention.
[13] R. L. Garwin, L. M. Lederman, and M. Weinrich, Phys. Rev. **105**, 1415 (1957); we use a modification developed here and discussed by R. A. Swanson, *ibid.* **112**, 580 (1958).
[14] R. D. Ehrlich, D. Fryberger, R. J. Powers, B. A. Sherwood, V. L. Telegdi, and J. Bounin, Phys. Rev. Letters **16**, 540 (1966).
[15] The carbon runs were performed with the same magnet configuration as in Ref. 8 which stopped pions; injection took place through low mass coils. The porthole was provided to increase the muon stop rate and the effective muon polarization (reduce the stopping pion admixture), two factors which were not relevant in Ref. 8.
[16] R. A. Lundy, Rev. Sci. Instr. **34**, 146 (1963). We used here a later version developed by T. A. Nunamaker.

(456)] passed through either of these gates; the spark chambers were then pulsed and the digitron stopped. When there was no trigger, the digitron was stopped and reset at the end of each gate. The time interval measured by the digitron was used to obtain the angle of the positron trajectory with respect to the precessed muon polarization. For each trigger, the relevant information (spark locations, digitron time interval, double-start/stop bits, and real and accidental tag bits) was written on magnetic tape for subsequent analysis on a large computer (IBM 7094).

Under typical conditions, using a Li target of 0.42 g/cm^2, the muon stop rate was 1.6×10^3/sec, the "positron" rate 5.2/sec, and the trigger rate 1.1/sec. For the stepped C target (effectively 0.84 g/cm^2 these rates were 1.8×10^3/sec, 4.5/sec, and 1.0/sec, respectively.

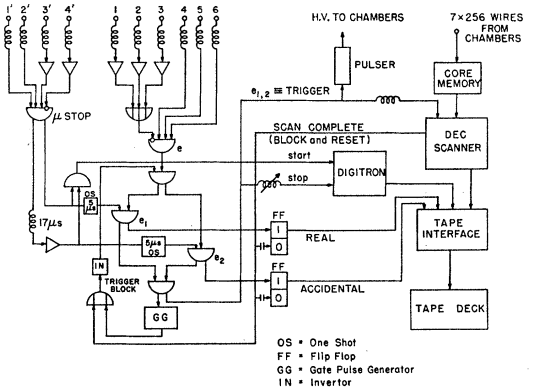

FIG. 3. Electronic logic for triggering wire spark chambers, controlling digitron, and labelling the events "real" or "accidental," and tape recording.

III. EXPERIMENTAL SPECTRUM

As a function of momentum x and time t, the event rate varies as

$$N(x,t)\sim e^{-\lambda t}\{1+A(x)\cos[\omega t-\phi(x)]\}\Omega(x), \qquad (2)$$

where $A(x)=P\xi B(x)/M(x)$ is the experimental asymmetry, ω the angular velocity of muon precession, λ the muon decay rate, $\Omega(x)$ the effective spectrometer solid angle, and $\phi(x)$ the (momentum-dependent) precession phase. It is evident from Eq. (2) that one may, after a decay correction (multiplying by $e^{+\lambda t}$), obtain $A(x)$ without knowing the momentum-dependent $\Omega(x)$. Hence the parameters of $A(x)$, δ governing the shape and $P\xi$ the magnitude, may also be found without knowing $\Omega(x)$; how the $\phi(x)$ was obtained is explained in Sec. V below. The magnetic field was chosen so that the events of the greatest statistical power for the determination of δ ($x\approx0.5$) fell where $\Omega(x)$ was the greatest.

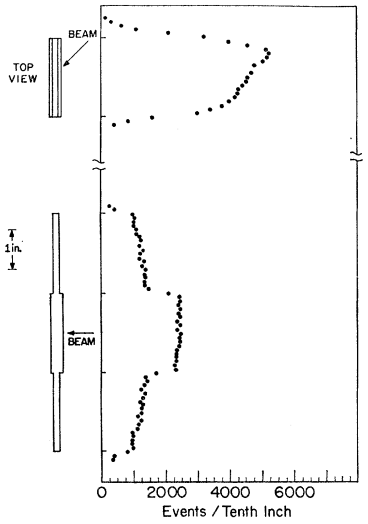

FIG. 2. Distributions of stops in the stepped graphite target. Appropriate target profiles are shown. The graphite density was measured to be 1.73 g/cm^3.

Real and accidental triggers in the momentum range of interest ($0.3\leq x\leq1.1$) were collected simultaneously. As anticipated, the accidental spectrum was flat in time and resembled the isotropic spectrum in momentum. After the application of all event selection criteria, it constituted typically $<1.5\%$ of the real spectrum. To obtain the final spectrum, the accidental spectrum was subtracted.

IV. EVENT-SELECTION CRITERIA

For a trigger to become a candidate for trajectory computation, we required at least one spark in each chamber. We also allowed up to two extra sparks (one in pitch and/or radius) choosing the sparks which yielded the best (least-squares fitted) helix; the details of the helix fitting procedure are given in Ref. 8.

Once having the trajectory, we imposed on it the following selection criteria: (1) that it emerged from a fiducial target inscribed in the physical one, but smaller than it by a 0.1-in peripheral "guard ring;" (2) that it entered a fiducial counter, similarly inscribed in counter 5 with a 0.25-in. guard ring; (3) that it cleared fiducial edges of the wire chambers, inside the physical edges by 0.25 in.; and (4) that it did not scatter "too much." The scatter in pitch was determined by extrapolating (a straight line) from chambers P1 and P2 to P3, the scatter in radius by extrapolating (a circle) from chambers R1, R2, and R3 to R4. The maximum allowed pitch scatter was 1 in. in P3; the corresponding maximum radial scatter (in R4) was equivalent to 0.04 x units of momentum. These limits are respectively 6 and 4.3 times the standard deviations of the corresponding scattering distributions.

The above fiducials, (1) through (3), were needed to compute the effective spectrometer solid angle. The location of these fiducials and the adequacy of the guard rings were verified from actual illumination plots.

TABLE II. Data, asymmetric spectrum.

Decile	x_i	Time bin 1	2	3	4	5	6	7	8	9
					Date set I[a]					
1	0.418	1498	1517	1618	1497	1602	1486	1576	1524	
2	0.474	1730	1733	1675	1616	1690	1764	1687	1610	
3	0.530	1762	1821	1839	1826	1908	1824	1905	1831	
4	0.586	1896	1905	1977	1902	1990	2036	1927	1853	
5	0.642	1908	1888	2026	2014	2140	2011	2000	1834	
6	0.698	1801	1781	1998	1971	2047	1991	1890	1803	
7	0.754	1497	1530	1703	1824	1985	1819	1760	1663	
8	0.810	1336	1399	1645	1765	1755	1688	1544	1382	
9	0.866	1175	1231	1370	1526	1655	1527	1369	1219	
10	0.922	976	959	1185	1352	1406	1317	1090	997	
					Data set II[a]					
1	0.418	1687	1775	1717	1673	1698	1701	1823	1763	
2	0.474	1831	1830	1898	1854	1919	1905	1891	1908	
3	0.530	2049	2019	2056	2032	2092	2036	2071	2034	
4	0.586	2106	2030	2147	2248	2284	2235	2178	2129	
5	0.642	2118	2206	2299	2286	2512	2285	2138	2139	
6	0.698	1922	1934	2156	2152	2395	2200	2007	1958	
7	0.754	1635	1662	1889	2096	2175	2072	1912	1738	
8	0.810	1457	1537	1718	1846	1947	1864	1645	1433	
9	0.866	1160	1377	1504	1707	1836	1667	1549	1217	
10	0.922	927	1013	1242	1411	1585	1430	1192	1000	
					Data set III[a]					
1	0.418	1376	1391	1344	1383	1412	1425	1453	1340	
2	0.474	1491	1526	1467	1524	1521	1511	1536	1540	
3	0.530	1650	1871	1781	1694	1693	1678	1643	1639	
4	0.586	1907	2019	2055	2016	1835	1743	1817	1745	
5	0.642	2006	2258	2173	2183	2027	1862	1786	1834	
6	0.698	2033	2239	2227	2191	1904	1628	1732	1819	
7	0.754	1863	2260	2325	2087	1775	1469	1383	1631	
8	0.810	1783	2037	2154	1968	1606	1332	1202	1354	
9	0.866	1541	1971	2007	1841	1441	1092	960	1131	
10	0.922	1345	1742	1884	1674	1245	809	703	889	
					Data set IV[a]					
1	0.35	724	684	669	683	651	663	714	684	715
2	0.41	807	813	822	777	760	746	750	853	808
3	0.47	959	926	1006	876	900	911	826	894	953
4	0.53	993	1008	1007	1050	1081	1082	1068	959	1016
5	0.59	949	1010	1090	1102	1107	1049	1041	1021	998
6	0.65	905	1012	1037	1045	1124	1039	1008	881	845
7	0.71	772	866	935	1044	1042	980	884	815	739
8	0.77	627	774	907	965	1019	973	789	661	643
9	0.83	566	657	823	901	908	836	709	559	493
10	0.89	396	549	710	800	830	755	610	491	360

[a] See Table IV for the experimental details.

The momentum range accepted for analysis was cutoff on both ends at points where the observed spectrum became highly momentum-dependent for experimental reasons. The lower cutoff (at a helix radius of about 27 in.), was based upon solid-angle considerations; the upper cutoff was set to exclude the spectrum "edge" (52.3 MeV/c).

Selection criteria in timing were also imposed. To avoid electronic event losses, e.g., by veto pulse reflections or trigger dead time, the first precession cycle (about 80 nsec) was discarded. Of the subsequent cycles an integral number (about 60) was retained for analysis.

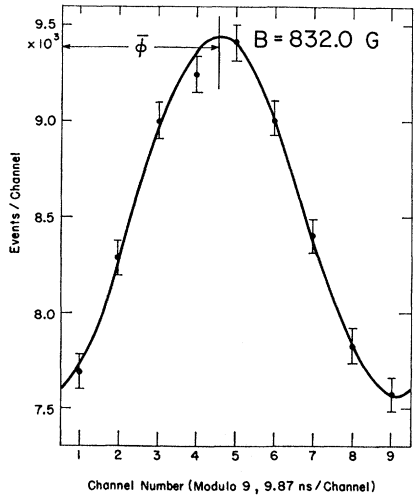

FIG. 4. Precession curve obtained by integrating data over momentum ($0.32 \leq x \leq 0.92$), folding (58 cycles) in time, and correcting for decay. The data here were obtained from a 0.42-g/cm² Li metal target in a field of 832 G. The sine curve fitted to this data has $\chi^2 = 3.8$ (6 degrees of freedom) and $\bar{\phi} = 2.85 \pm 0.06$.

V. ANALYSIS

A. Asymmetric Spectrum

For the purposes of analysis, the data from any given run were grouped into deciles, i.e., into ten equal momentum bins about (mean) momenta x_i. For each decile, a corresponding asymmetry $A_i(x_i)$ (datum point) was computed. The parameters δ and $P\xi$ were then determined by fitting (minimum χ^2) predicted asymmetry functions $\tilde{A}(x; \delta, P\xi)$ to the A_i.

The functions $\tilde{A}$ were derived from theoretical (radiatively corrected[17]) spectra M and B; in computing M, the assumptions $\rho = \frac{3}{4}$ and $\eta = 0$ were made. Functions $\tilde{M}$ and $\tilde{B}$ were computed from M and B by folding in (a) the effects of energy losses (in the target and in counters 3 and 4) due to both ionization[18] and radiation,[19] and (b) the spectrometer resolution function. This latter function was derived from the data proper by comparing the observed scattering distributions to Monte Carlo calculations.[8] The predicted asymmetry $\tilde{A}_i$ is the quotient $P\xi \int \tilde{B} dx / \int \tilde{M} dx$ where the integrations are performed over the ith decile.

The precession and digitron frequencies had been so chosen that one muon precession cycle fell exactly in an integral number k (in practice 8 or 9) of digitron time bins. Hence the asymmetries A_i could be conveniently computed from data obtained by adding up successive time bins modulo k, i.e., by folding all precession cycles (about 60) onto a single one. The decay correction [see Eq.(2)] (applied to this single cycle) is small, viz., at most of the order $\pi\lambda/\omega \approx 2\%$. Table II gives the experimental asymmetry data, after time folding and the decay correction.

The mean precession phase angle $\bar{\phi}$ was determined from a precession curve integrated over all momenta

[17] The radiative corrections which were used here were those computed for V and A interactions (two-component neutrino theory). While it is technically not proper to treat the interaction as a general one and correct with less general radiative corrections, one is forced to do so because the general corrections do not converge [see R. E. Behrends, R. J. Finkelstein, and A. Sirlin, Phys. Rev. **101**, 866 (1956)]. There is, however, at least the mitigation that the results of muon-decay experiments are consistent with two-component neutrino theory.

[18] Using the experimental distribution for 15.7-MeV electrons of E. L. Goldwasser, F. E. Mills, and A. O. Hanson, Phys. Rev. **88**, 1137 (1952). The low-energy tail of this distribution was extended according to the E^{-2} dependence derived by Landau.

[19] W. Heitler, *The Quantum Theory of Radiation* (Oxford University Press, New York, 1954), 3rd ed., p. 242.

TABLE III. Data, isotropic spectrum.

Decile	x^i	Data set V[a] ($\frac{1}{4}$ in. carbon) N_{expt}	N_{theor}	$(N_{expt}-N_{theor})/\sqrt{N_{theor}}$	Data set VI[a] ($\frac{1}{8}$ in. carbon) N_{expt}	N_{theor}	$(N_{expt}-N_{theor})/\sqrt{N_{theor}}$
1	0.465	8538	8672	−1.44	7555	7480	0.87
2	0.515	9378	9381	−0.03	8141	8143	−0.03
3	0.565	10092	10102	−0.10	8731	8821	−0.96
4	0.615	10723	10697	0.25	9272	9391	−1.23
5	0.665	10564	10586	−0.22	9369	9344	0.26
6	0.715	10028	9882	1.47	8832	8773	0.63
7	0.765	9216	9092	1.26	8098	8125	−0.30
8	0.815	8137	8276	−1.53	7505	7442	0.72
9	0.865	7531	7422	1.27	6789	6727	0.76
10	0.915	6389	6482	−1.16	5916	5962	−0.59

[a] See Table IV for experimental details.

(Fig. 4). The value of $\bar{\phi}$ is governed by two factors: (1) the orientation of the mean polarization **P** when the muon stops, and (2) the precession angle excluded from the analysis (which does not start at $t=0$). The "mean" momentum assigned to $\bar{\phi}$ is defined by $\bar{x}=\sum_i x_i B_i \Omega_i / \sum_i B_i \Omega_i$; we had for the 1000-G runs $\bar{x}=0.75$, and $\bar{x}=0.68$ for the 832-G run. The deduced value of δ is insensitive to errors in $\bar{\phi}$; all the A_i are merely multiplied by $\cos\Delta\bar{\phi}$ (as is the deduced value for $P\xi$), where $\Delta\bar{\phi}$ is the error in the mean phase angle.

Two estimates of the decile phase shifts ($\bar{\phi}_i$ and ϕ_i) were made. Elementary orbit theory predicts that $\bar{\phi}_i=\bar{\phi}+\text{arc sin}(d/2R_i)-\text{arc sin}\ (d/2\bar{R})$, where d is the distance between the target and final counter, and R denotes helix radius. For each decile, distributions of takeoff angle were obtained from the trajectory information. The means of these distributions, ϕ_i, agreed with the $\bar{\phi}_i$ to within $|\phi_i-\bar{\phi}_i|\leq 10^{-2}$ rad. We therefore expect that the errors $\Delta\phi_i$ are of this order; the associated error in the A_i goes like $(1-\cos\Delta\phi_i)$ which is quite small.

The use of $\bar{\phi}$ and ϕ_i in the extraction of the experimental decile asymmetry by means of Fourier analysis is shown in Appendix B. This Fourier technique is much faster (computationally) than a least-squares technique, and for the asymmetries typical of this data (<0.5) is as powerful statistically.

B. Isotropic Spectrum

In order to gain additional understanding of the apparatus and to lay a foundation for future, more accurate, muon decay experiments, the isotropic portion of the spectrum was also analyzed.[20] This analysis required, in addition to the corrections made to the asymmetric spectrum, the evaluation of certain momentum-dependent functions which were not relevant to that analysis. The most significant of these functions is the effective solid angle $\Omega(x)$.

The nature of the solid angle which characterizes this spectrometer differs from that of traditional spectrometers in one important aspect, viz., the mean direction of the bundle of trajectories accepted into $\Omega(x)$ from any given source (target) point varies considerably with momentum. As x goes from 0.4 to 1, this direction changes by about 30°; since the detector (final counter) subtends about 6° at the source, there is little overlap of these bundles for different momenta. The details of the solid angle calculation are given in Appendix C. A plot of $\Omega(x)$ is given in Fig. 5.

Two other possible sources for momentum-dependent corrections were also considered: annihilation in flight, and δ-ray production in the target; these are discussed below under systematics.

To obtain the input for the isotropic spectrum, it is sufficient to add up (for each decile) the time-folded precession cycle, thus averaging out the asymmetry; this procedure is correct provided that the decay correction is applied *before* adding up the data in the cycle. Table III lists the isotropic data points obtained by this procedure, as well as best-fitting predicted values $\tilde{M}\Omega$.

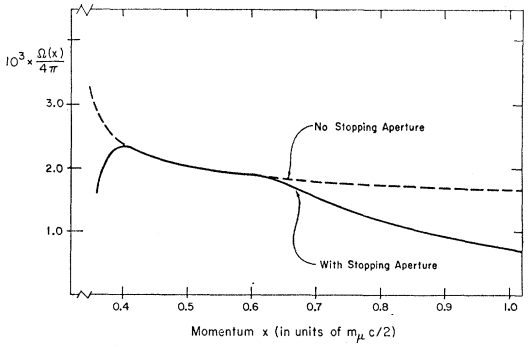

FIG. 5. A solid-angle plot for 1000 G. The drop in solid angle at the lower end is due to stopping by the outside edges of chambers R3 and P2 while that at the upper end is due to their inside edges. The dashed lines indicate the solid angle without the aperture stop of the chamber edges.

[20] All of the data was not used in this analysis because of a temporary minor malfunction in the DEC scanner. This malfunction resulted in a chamber inefficiency of about 2% (sets of effectively dead wires were occurred throughout the spectrometer) and was quite evident in the chamber illumination plots. While this effective [chamber] inefficiency lead to no errors in the determination of the correct A_i, it did make the explicit computation of $\Omega(x)$ too complicated to be reliable or worthwhile. Hence the analyses requiring $\Omega(x)$ were done only on that part of the data which was taken before the scanning difficulties began.

TABLE IV. Experimental results.

Data set	Field (G)	Target material (g/cm²)	Source thickness[a] (10^3 radiation lengths)	Momentum bite	Number of events (10^3)	δ	$P\xi$	χ^{2b}
			Asymmetric spectrum					
I	1000	C 1.10	18	0.39–0.95	147.8	0.788±0.024	0.36	6.26
II	1000	C 0.55	10	0.39–0.95	133.8	0.738±0.028	0.34	6.73
III	1000	Li 0.40	5.6	0.39–0.95	134.5	0.750±0.012	0.71	7.97
IV	832	Li 0.42	5.7	0.32–0.92	76.5	0.744±0.017	0.66	3.89
					Weighted mean	0.752±0.008$_8$		
			Isotropic spectrum					
						$\rho(\eta\equiv 0)$	$\eta(\rho\equiv\frac{3}{4})$	χ^{2b}
V	1000	C 1.10	18	0.44–0.94	90.6	0.757±0.007$_5$	−0.61±0.41	11.2
VI	1000	C 0.55	10	0.44–0.94	80.2	0.767±0.007$_8$	−0.90±0.42	5.1
					Weighted mean	0.762±0.005$_3$		

[a] Includes scintillator 4, deadlayer in scintillator 3, and scintillator wrappings (one layer 0.5 mil aluminized Mylar, one layer 0.5 mil aluminum).
[b] For 8 degrees of freedom.

VI. RESULTS

The details of the best fits (to data points A_i) for δ and $P\xi$ and those for ρ and η (fits to $M_i\Omega_i$) are given in Table IV. These fits were done after corrections for all known systematic effects had been made, and hence represent the best estimates of these parameters. The quoted errors are statistical standard deviations. Figure 6 is a plot of the asymmetry points A_i observed with the Li target, together with the best-fitting theoretical curve $\tilde{A}(x;\delta,P\xi)/P\xi$. The observed isotropic spectrum (corrected for solid angle) and the best-fitting $\tilde{M}$ are shown in Fig. 7.

Systematic Errors

The systematic corrections in this experiment may be grouped into three categories: effective solid angle, timing, and momentum scale. Summaries of these corrections are given in Table V.

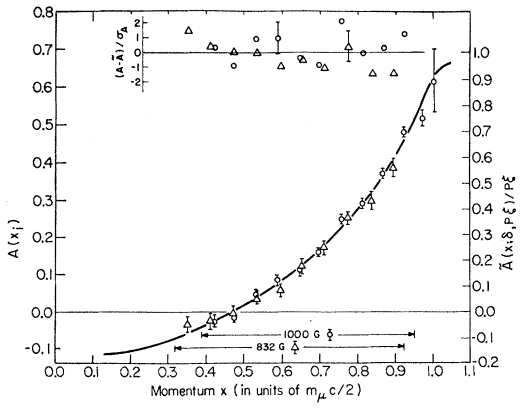

FIG. 6. Experimental asymmetries A_i observed with the Li targets. The solid line is a best fitting theoretically predicted curve (including corrections) to this data ($\delta=0.748$ and $P\xi=0.69$, (see Table IV). This curve extends above $x=1$ due to finite spectrometer resolution. Each datum in the regions of fit is replotted on the scatter plot at the top of the figure.

Factors which may be placed in the first category, besides $\Omega(x)$, include positron annihilation in flight, cancellation of event analysis by δ rays (multiple sparks), chamber inefficiencies, and event loss due to scattering. While this category is not relevant to the analysis of the asymmetric spectrum, these factors had to be evaluated and used in the analysis of the isotropic spectrum.

As a consistency check, a portion of asymmetric data was analyzed twice: first, by fitting to A_i and second, by fitting to $B_i\Omega_i$ (using the above solid-angle factors). These two analyses yielded identical results both in χ^2 and in the deduced values of δ and $P\xi$, indicating that the computation of Ω and the solid-angle corrections were not in error. Unfortunately, this check is not as sensitive as one might think, because the asymmetric spectrum contains a crossover (near $x=\frac{1}{2}$), a *qualitative* difference in functional form from first-order errors in solid-angle "shape." As an example of this insensitivity, the systematic error in $\delta(\tilde{B}\Omega$ fits) due to uncertainties (induced by errors in target coordinates) is an order of magnitude smaller than the analogous one in $\rho(\tilde{M}\Omega$ fits, $\eta\equiv 0$). The only solid-angle error associated with the values of δ and $P\xi$ (from $\tilde{A}$ fits) comes from the assigned values of ρ and η, and because of the crossover, this error is small.

The momentum dependence of event loss due to annihilation in flight[21] was calculated allowing for 7% of scintillator 3, 50% of the target, all of scintillators 4 and 5, all of the wires, gas, etc. in the spectrometer, and 50% of scintillator 6.

Cancellation of events by δ rays from the target required no correction because it was both small and momentum-independent. Events are in fact cancelled only if there is more than one spurious spark in pitch or radius; the δ-ray momentum threshold for this to occur (for a δ ray to reach chamber R2) is 5 MeV.

[21] J. M. Jauch and F. Rohrlich, *The Theory of Photons and Electrons* (Addison-Wesley Publishing Co., Inc., Reading, Mass., 1965), p. 269.

The probability for the creation of a 5 MeV (or greater) δ ray in the target is $<1\%$.

From results of prior experiments the chambers were known to be highly efficient; typical inefficiencies[8] were 0.2%. Even if this inefficiency were distributed in a most detrimental (but highly unlikely) way, viz., varying linearly from 0 to 0.4% across a chamber, then its maximum effect on ρ would be $\Delta\rho=0.0004$.

The errors in ρ due to scattering were studied by varying the scattering cutoffs for event trajectory selection, and by doubling the fiducial guard-ring widths. No systematic effects were observed when these cutoff values were increased or decreased by a factor of two, and none were observed as the widths were doubled.

Only the asymmetric spectrum is susceptible to time-scale errors. The digitron was checked in the manner described by Weber *et al.*[22] and Lundy[23] against incremental nonlinearity by accumulating a spectrum of 5×10^5 random events. This spectrum was flat, checking the individual bin sizes to 3%. When added modulo 8 or modulo 9 the spectrum was still flat checking to 0.25% the relevant systematic incremental nonlinearities. Due to the relatively short precession period, the experimental results are relatively insensitive to long-term (say 1 μsec) time irregularities. In fact, a uniform stretching of the time scale will not affect δ, but merely decreases $P\xi$. As a check of digitron performance against long-term errors a muon lifetime was deduced from the data ($\sim10^5$ events). The result was 2.204 ± 0.008 μsec with a $\chi^2=57.5$ for 58 degrees of freedom, in agreement with the known lifetime and precluding any long-term timing errors. Since the digitron was operated in a severe interference environment (spark noise), several checks were made to test the digitron against short-term errors (i.e., of order $2\pi/\omega$). A "no-sparks" run was taken and the total asymmetry (obviously no momentum information was available) was found to be the same (within statistics) as in the normal runs. In addition, data were taken with several different digitron stop delays; this causes shifts in $\bar{\phi}$. By distributing these $\bar{\phi}$'s throughout the precession cycle, possible systematic nonlinearities of time scale (e.g., those due to unbalanced flip-flop operation) were averaged out. The data sets of different $\bar{\phi}$ were analyzed separately and gave consistent results. The most significant data for the asymmetry measurement (Li) were taken in approximately equal amounts with an even (8 bins, 1000 G) and an odd (9 bins, 832 G) number of time bins per precession cycle. The results were consistent and the precession χ^2's were reasonable (e.g., Fig. 4); again there was no evidence of any systematic timing error. The only timing-associated corrections necessary were those for the phase angle

TABLE V. Systematic effects.

Symmetric effect	$10^3\,\Delta\delta$[a]	Estimated uncertainty ($\pm$) in $10^3\,\Delta\delta$
Assigned values ρ and η[b]	...	0.8
Absolute momentum scale	1.7	1.5
Ionization loss (Landau) tail	2.3	0.4
Bremsstrahlung tail	6.8	0.8
Muon depolarization in scintillator	−1.5	0.2
Intrinsic spectrometer resolution	−0.2	0.05
Phase angle relation in spectrometer	3.7	0.1
Total systematic uncertainty[c]	...	1.95
	$10^3\,\Delta\rho$ ($\eta\equiv0$)[a]	Estimated uncertainty ($\pm$) in $10^3\,\Delta\rho$
Absolute momentum scale	1.7	2.0
Ionization loss (Landau) tail	7.0	2.0
Bremsstrahlung tail	20.0	3.5
Annihilation in flight	−3.1	1.0
Spark-chamber inefficiency	...	0.5
Illumination centroid location	...	0.5
Intrinsic spectrometer resolution	7.0	1.5
Total systematic uncertainty[c]	...	5.0

[a] The magnitude of the systematic effect is found by weighting that of each data set with its statistical weight. The sign is defined by, e.g., $\Delta\delta=\delta$ (after correction) $-\delta$ (before correction).
[b] Taken as a correlated pair.
[c] The total uncertainty is found by quadrature addition.

and the decay rate. The uncertainty in the latter is negligible.

The remainder of the systematic corrections are all momentum associated. While the spectrometer could, in principle, be used to measure momenta absolutely, we chose instead (as in Ref. 8) to use the data, in particular, the observed endpoint locations, to calibrate the momentum scale. The endpoint was observed at four fields ranging from 0.832 to 2.1 kG, enabling calibration throughout the range of accepted radii. The observed locations were all consistent with each other and very close to their predicted positions. These observations led to a shift of the momentum scale by 0.0017 x units. This shift corrects at once for all systematic effects

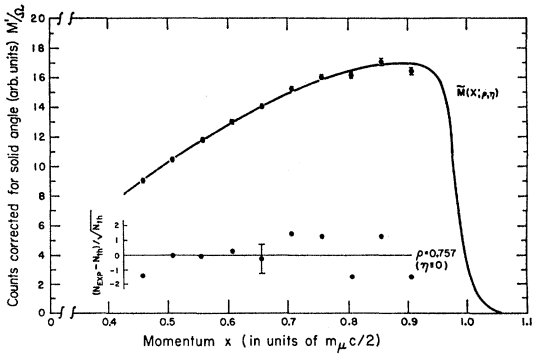

FIG. 7. Data points of the observed isotropic spectrum M' (taken with the $\frac{1}{4}$-in. C target) with the momentum dependence of the solid angle (see Fig. 5) removed. The region of fit was $0.44\leq x\leq0.94$; the lower limit was set above the spark-chamber occultation region. The solid curve is the best-fitting theoretically predicted curve to this data. Each datum is replotted on the scatter plot at the bottom of the figure.

[22] W. Weber, C. W. Johnstone, and L. Cranberg, Rev. Sci. Instr. **27**, 166 (1956).
[23] R. A. Lundy, Phys. Rev. **125**, 1686 (1962).

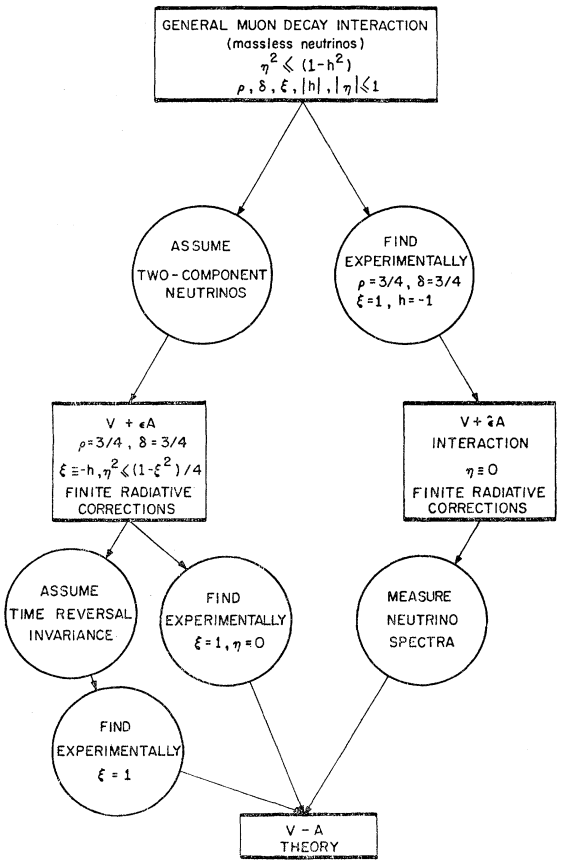

FIG. 8. Logical diagram of relationships and hypotheses of muon decay.

affecting that scale, e.g., uncertainties in chamber locations, clearing field shifts, energy-loss errors, etc.

To check the energy-loss corrections, the data were taken for several target thicknesses and types, and the edge locations and shapes were recorded. The mean losses and observed shapes were all found to be consistent and in agreement with theoretical predictions. This remark is particularly pertinent to the carbon data, since these were taken with a stepped target (see Fig. 2).

A rather small and somewhat subtle correction is required because the electrons in the isotropic (M) and anisotropic (B) parts of the spectrum undergo slightly different energy losses upon leaving their source. This source consists in fact not only of the target, but also of those "dead" surface layers of scintillators 3 and 4 where insufficient light is produced to guarantee perfect veto efficiency. Inasmuch as the muons get greatly depolarized in scintillating plastic (to about 0.3 of P, see R. A. Swanson, Ref. 13), events from these layers contribute only partially to B, but fully to M. From the illumination plots (Fig. 2) one finds that about 10% of all events come from these dead layers, corresponding to a total (scintillator) thickness of about 20 mil. Allowing for the high specific ionization of stopping muons compared to that of relativistic electrons, 4 mil of these are allocated to counter 4, and 16 mil to counter 3.

The systematic corrections large enough to be significant, and conservative estimates of their uncertainties, are given in Table V. From Tables IV and V, it is evident that the systematic uncertainties in δ, as compared to the statistical ones, are almost negligible; the accuracy of δ could hence be considerably increased by merely collecting additional data. Further improvements could be realized by reducing the uncertainties in the major systematic corrections. For two of these this would be relatively easy to do: The momentum scale uncertainty could be reduced by acquiring more data on the endpoint locations; the uncertainty associated with the measurement errors in ρ and η could be eliminated by fitting to $B_i\Omega_i$ directly. In the latter case the uncertainties due to errors in Ω could be kept small (recall that δ is relatively insensitive to errors in Ω) by taking additional precautions not required for the goals of this experiment (in particular eliminating the "aperture" effect). The error in δ could be reduced by a factor of 4 to 5 by taking these steps, but many more events ($\sim 10^7$) and a new spectrometer would be required.

Adding (in quadrature) the systematic and the statistical uncertainties yields the following final results:

$$\delta = 0.752 \pm 0.009,$$

and

$$\rho = 0.762 \pm 0.008 \quad (\eta \equiv 0),$$

or

$$\eta = -0.7 \pm 0.5 \quad (\rho \equiv \tfrac{3}{4}),$$

which are consistent with the predictions of the two-component neutrino theory. Note that using the above values of ρ and η (instead of $\frac{3}{4}$ and 0) in the analysis of the asymmetric spectrum results in a negligible shift (about -0.001) in the deduced value of δ.

The above results, combined with averages of the most reliable experimental muon decay parameters, indicate (when analyzed following the work of Jarlskog,[7] see Appendix A) that the interaction (in charge retention order) may still include as much as 30% of scalar, pseudoscalar, or tensor couplings. These limits are obviously still too large[24] to declare with confidence that muon decay is a V and A interaction.

VII. FUTURE EXPERIMENTS

Of the parameters of muon decay, the electron helicity h and the low-energy shape parameters η of the isotropic spectrum are at present the least accurately known. It is of interest to inquire as to which of these

[24] Since experimental data with smaller errors are now available, one might expect these limits to be smaller than those quoted in Ref. 7. This is not the case due to a numerical error [C. Jarlskog, (private communication)].

parameters is more significant for determining the nature of the decay interaction, i.e., which should be determined with greater accuracy first.

An answer to this question cannot be given without specifying the framework of hypotheses in which one chooses to operate. The somewhat complicated relationships between various assumptions about the decay interaction and their implications (already discussed in Sec. I) are illustrated in Fig. 8.[25] The right-hand side of this logical diagram corresponds to the general analysis approach of Jarlskog,[7] the other to the *postulate* of 2-component neutrinos.

Let us first consider this latter approach; it clearly could not be justified without reference to semileptonic processes. If one adds the further postulate of time-reversal invariance, then ϵ is real. The parameters η and ξ ($\equiv -h$) depend quadratically on ϵ; this dependence is such that to determine ϵ (with its sign), both of them have to be measured, unless $\xi=1$. Recently, the very accurate value ($\xi=0.975\pm0.015$) has become available.[26] While consistent with $\xi=1$, this value implies only $\epsilon=-1.25\pm0.09$ or $\epsilon=-0.80\pm0.06$. A measurement of η to ~0.1 would be needed to resolve the ambiguity. A determination of h, to be useful, would have to be more accurate than the recent ξ value. If T invariance is not postulated, then ϵ is complex and obviously both η and ξ have to be determined.

In the framework of the general analysis approach, it is most useful to measure h accurately. As we show in Appendix A, the currently admissible S, T, and P "contaminations" are essentially entirely due to the present uncertainty in h. In this scheme, η serves only as consistency check for the relation $\eta^2\leq(1-h^2)$ which holds quite generally.

Hypothetical experiments in which decay spectra are measured for *specified* electron polarizations (each yielding a parameter set ρ', ξ', etc.) have been discussed.[27] These discussions show however that these additional parameters still do not determine the coupling constants unambiguously. It is further evident that the known *large* decay electron helicity (longitudinal polarization) increases the difficulty in measuring these additional parameters; unit electron helicity would altogether preclude their measurement. The general analysis detailed above applies in this latter case.

[25] This diagram evolved from a series of discussions with V. L. Telegdi.

[26] I. I. Gurevich, L. A. Makariyna, B. A. Nikol'sky, B. V. Sokolov, L. V. Surkova, S. Kh. Khakimov, V. D. Shestakov, Yu. P. Dobretsov, and V. V. Akhmanov, Phys. Letters **11**, 185 (1964). A more recent, more accurate result is reported (in Russian) by I. I. Gurevich, L. A. Makariyna, A. P. Mishakova, B. A. Nikol'sky, B. V. Sokolov, L. V. Surkova, V. D. Shestakov, V. V. Akhmanov, and Yu. P. Dobretsov, I. V. Kurchatova Atomic Energy Institute, Moscow, Report IAE 1297, 1967 (unpublished).

[27] T. Kinoshita and A. Sirlin, Phys. Rev. **108**, 844 (1957). A communication on this subject was also presented by L. Michel and F. Bourdelet at the Padua Venice Conference, 1957 (unpublished).

ACKNOWLEDGMENTS

I wish to thank Professor V. L. Telegdi for suggesting this project. His insight and generous assistance have helped me through its particularly difficult portions.

I thank my collaborators, R. Ehrlich, D. Jensen, C. Nissim-Sabat, R. Powers, and B. Sherwood for contributing a great deal of their time, effort, and thought toward the completion of this project. In particular, I wish to thank B. Sherwood for helpful discussions and important contributions to the design of the experiment and to the data analysis. I thank R. Swanson, K. Sebesta, T. Shea, and J. Horton for technical assistance. I am indebted to J. Bounin and R. Norton for generously giving their engineering skills. Finally I with to acknowledge useful correspondence from Dr. C. Jarlskog.

APPENDIX A: EXPERIMENTAL LIMITATIONS OF THE COUPLING CONSTANTS

To understand the relationships between the decay parameters and the coupling constants, it is useful to consider the Hamiltonian written out in three different orderings, viz.,

$$\tilde{H}(CC)=\sum_i (\bar{e}\Gamma_i\nu_e)(\bar{\nu}_\mu\Gamma_i(\tilde{C}_i+\tilde{C}_i'\gamma_5)\mu)+\text{H.c.}, \quad \text{(A1)}$$

$$H(CR)=\sum_i (\bar{e}\Gamma_i\mu)(\bar{\nu}_\mu\Gamma_i(C_i+C_i'\gamma_5)\nu_e)+\text{H.c.}, \quad \text{(A2)}$$

and

$$\hat{H}(CJ)=\sum_i (\bar{e}(\hat{C}_i+\hat{C}'\gamma_5)\Gamma_i\mu)(\bar{\nu}_\mu\Gamma_i\nu_e)+\text{H.c.}, \quad \text{(A3)}$$

where $i=S$, V, T, A, and P stand for the type of coupling, Γ_i are the corresponding operators (1, γ_μ, $\sigma_{\mu\nu}$, $i\gamma_\mu\gamma_5$, γ_5), and the C_i, C_i', etc. are coupling constants (the tilde and the caret denote the orderings). The first ordering is in the form of a current-current interaction, and analog of that commonly used to describe β decay; the second is the so-called charge-rentention form; and the third (also a charge-retention ordering) was used by Jarlskog[7] to obtain simpler relationships between the coupling constants and the decay parameters.

These Hamiltonians are equivalent,[28] i.e., a given set of coupling constants in one ordering is linearly related (by a so-called Fierz-Michel transformation) to that in another. These transformations are such that if the interaction is $V-A$ in one ordering, it is $V-A$ in all three. A general V and A coupling in Eq. (A3), which Jarlskog has shown would be implied by experimentally verifying the so-called "$V-A$ predictions" of the *practically* observable parameters (i.e., $\rho=\delta=\frac{3}{4}$; $\xi=-h=1$), implies a V and A coupling in Eq. (A2). However, a

[28] See, for example G. Källén, *Elementary Particle Physics* (Addison-Wesley Publishing Co., Inc., Reading, Mass., 1964), p. 377.

$V+A$ coupling in Eq. (A3) corresponds to $S-P$ in the CC ordering. Hence, the limitation to V and A couplings in the Jarlskog form [Eq. (A3)], which may be denoted as a $V+\hat{\epsilon}A$ interaction where $\hat{\epsilon}=\hat{C}_A/\hat{C}_V$, will lead to an $S-P$ admixture to the interaction written in the current-current form. Specifically, the most general CC interaction compatible with the $V-A$ values of the practically observable decay parameters can be written symbolically as $\frac{1}{2}(\hat{\epsilon}-1)(V-A)+(\hat{\epsilon}+1)(S-P)$.

Let us now compare two hypotheses which restrict the Hamiltonian: (a) assuming the observable decay parameters to have their "$V-A$" values, or (b) assuming two-component neutrinos.[29] The resulting restricted Hamiltonians (CR or CJ), though both V and A, are *not* equivalent; the relationships between the parity-conserving and parity-violating terms differ, i.e., (a) leads to $C_V'=-C_A$ and $C_A'=-C_V$ where C_V and C_A are free, while (b) leads to $C_V'=\pm C_V$ and $C_A'=\pm C_A$, where again C_V and C_A are free; the upper (lower) sign refers to left (right)-handed neutrinos.

In the framework of (a), $\eta=0$ is automatically implied and thus does not further restrict the interaction. Its measurement furnishes a consistency check supplementing the measurements of the other parameters. More cannot be said about the interaction unless experiments measuring the neutrino spectra are performed (as suggested in Ref. 7) or additional hypothesis are imposed, e.g., (b) above. In the framework of (b) without time reversal invariance (T), $\rho=\delta=\frac{3}{4}$, and measurements of $\xi=-h$ and η will unambiguously determine the interaction,[30] viz., $\mathrm{Re}\epsilon=\xi/(2\eta-1)$ and $\mathrm{Im}\epsilon=[(1-2\eta)/(1+2\eta)-\xi^2/(2\eta-1)^2]^{1/2}$, where $\epsilon=C_A/C_V$. If T is assumed to be good, then ϵ is real and given by $\epsilon=[-1\pm(1-\xi^2)^{1/2}]/\xi$ or $=\pm[(1+2\eta)/(1-2\eta)]^{1/2}$; both ξ and η are required to resolve the ambiguity.

Using the Hamiltonian of Eq. (A3), Jarlskog has shown that

$$\rho 16g^2=3(a_2+a_4)+6a_3\,, \tag{A4}$$

$$3\alpha 16g^2=3(c_1+c_5)+4(c_2+c_4)-14c_3\,, \tag{A5}$$

$$\beta 16g^2=3(c_2+c_4)-6c_3\,, \tag{A6}$$

and

$$h16g^2=c_1+c_5+4(c_2+c_4)+6c_3\,, \tag{A7}$$

where

$$a_i\equiv\hat{C}_i^*\hat{C}_i+\hat{C}_i'^*\hat{C}_i'\,, \tag{A8}$$
$$c_i\equiv\hat{C}_i^*\hat{C}_i'+\hat{C}_i'^*\hat{C}_i\,,$$

and

$$16g^2\equiv a_1+a_5+4(a_2+a_4)+6a_3\,. \tag{A9}$$

The α and β are related to ξ and δ by

$$\xi=-3\alpha$$
and
$$\delta=\beta/3\alpha\,. \tag{A10}$$

The analogous result for η is easily found by using the results of Bouchiat and Michel[1] which convert by the Fierz-Michel transformation to

$$16g^2\eta=(|\hat{C}_1|^2-|\hat{C}_1'|^2)-(|\hat{C}_5|^2-|\hat{C}_5'|^2)$$
$$-2[(|\hat{C}_2|^2-|\hat{C}_2'|^2)-(|\hat{C}_4|^2-|\hat{C}_4'|^2)]\,. \tag{A11}$$

Following Jarlskog, we expand the parameters about specific values, i.e., set $\rho=\rho_0+\Delta\rho$, etc. Choosing these specific values to be those predicted by the $V-A$ theory one obtains

$$(64/3)g^2\Delta\rho=2a_3-a_1-a_5\,, \tag{A12}$$

$$16g^2(3\Delta\alpha)=3(c_1+c_5)+4(c_2+c_4)-14c_3+a_1+a_5$$
$$+4(a_2+a_4)+6a_3\,, \tag{A13}$$

$$(64/3)g^2\Delta\beta=a_1+a_5+4(a_2+c_2)+4(a_4+c_4)$$
$$+6(a_3-c_3)-2c_3\,, \tag{A14}$$

$$16g^2\Delta h=(a_1+c_1)+(a_5+c_5)+4(a_2+c_2)$$
$$+4(a_4+c_4)+6(a_3+c_3)\,, \tag{A15}$$

and

$$16g^2\Delta\eta=(|\hat{C}_1|^2-|\hat{C}_1'|^2)-(|\hat{C}_5|^2-|\hat{C}_5'|^2)$$
$$-2[(|\hat{C}_2|^2-|\hat{C}_2'|^2)-(|\hat{C}_4|^2-|\hat{C}_4'|^2)]\,. \tag{A16}$$

One notes that since

$$|\hat{C}_S|^2+|\hat{C}_S'|^2=a_1\equiv\bar{S}^2\,,$$
$$|C_S\pm C_S'|^2=a_1\pm c_1\equiv S_\pm^2\,,\ \text{etc.}\,, \tag{A17}$$

it is useful to find expressions either without the c_i or in which the c_i are paired with the a_i. It can be seen that the equation for $\Delta\eta$ does not allow this grouping and hence it is not used in the following analysis; it is included here for the sake of completeness. In addition, by using Eqs. (A15) and (A16), the general limitation imposed upon η by the helicity can be shown to be $\eta^2\leq(1-h^2)$. On the other hand, if $\eta=0$ (the $V-A$ prediction), it implies nothing about the other parameters.

Taking appropriate linear combinations of Eqs. (A12) through (A14), one obtains

$$(64/3)g^2(\Delta\rho+\Delta\beta)=4(a_2+c_2)$$
$$+4(a_4+c_4)+8(a_3-c_3) \tag{A18}$$

and

$$(16/3)g^2(\pm4\Delta\rho-\tfrac{4}{3}\Delta\beta-3\Delta\alpha)=\mp[(a_1\pm c_1)$$
$$+(a_5\pm c_5)-2(a_3\pm c_3)]\,. \tag{A19}$$

Equations (A12), (A15), (A18), and (A19) can be combined to yield

$$(64/3)g^2\Delta\rho=-(\bar{S}^2+\bar{P}^2)+2\bar{T}^2$$

[29] A. Salam, Nuovo Cimento **5**, 299 (1957); L. Landau, Nucl. Phys. **3**, 127 (1957); T. D. Lee and C. N. Yang, Phys. Rev. **105**, 1671 (1957).

[30] These solutions for ϵ are easily obtained from the equations for ξ and η found in Ref. 14. See also V. L. Telegdi, in Proceedings of the International Conference on Weak Interactions, Argonne National Laboratory Report No. ANL-7130, 1965, pp. 337–356 (unpublished).

and

$$(64/3)g^2(\tfrac{3}{4}\Delta h-\tfrac{3}{4}\Delta\alpha+\tfrac{4}{3}\Delta\beta)=2(\bar{S}^2+\bar{P}^2)+8(V_+^2+A_+^2)+12\bar{T}^2. \quad \text{(A20)}$$

Equations (A20) have the solution

$$\bar{S}^2+\bar{P}^2=(8/3)g^2[\tfrac{3}{4}\Delta h-6\Delta\rho-\tfrac{3}{4}\Delta\alpha+\tfrac{4}{3}\Delta\beta]-(V_+^2+A_+^2)$$

and (A21)

$$\bar{T}^2=\tfrac{4}{3}g^2[\tfrac{3}{4}\Delta h+2\Delta\rho-\tfrac{3}{4}\Delta\alpha+\tfrac{4}{3}\Delta\beta]-\tfrac{1}{2}(V_+^2+A_+^2).$$

Using Eqs. (A10) in the form (to first order)

$$3\Delta\alpha=-\Delta\xi, \qquad \Delta\beta=-\xi_0\Delta\delta-\delta_0\Delta\xi \quad \text{(A22)}$$

converts Eqs. (A21) to

$$\bar{S}^2+\bar{P}^2=(8/3)g^2[\tfrac{3}{4}\Delta h-6\Delta\rho-\tfrac{3}{4}\Delta\xi+\tfrac{4}{3}\Delta\delta]-(V_+^2+A_+^2),$$
$$\bar{T}^2=\tfrac{4}{3}g^2[\tfrac{3}{4}\Delta h+2\Delta\rho-\tfrac{3}{4}\Delta\xi+\tfrac{4}{3}\Delta\delta]-\tfrac{1}{2}(V_+^2+A_+^2). \quad \text{(A23)}$$

Equations (A23) have the meaning that if the parameters ρ, ξ, δ, and h (and hence $\Delta\rho$, etc.) were known precisely (not necessarily assuming the "$V-A$" values), then the quantities $(\bar{S}^2+\bar{P}^2)$ and $\bar{T}^2$ could be evaluated (assuming $V_+^2+A_+^2$ were also known). It can be seen that an analogous equation for $\bar{V}^2+\bar{A}^2$ cannot be found because there is no way to form $(V_-^2+A_-^2)$ or $\bar{V}^2+\bar{A}^2$) from the right-hand sides of Eqs. (A12) through (A16).

At this point one can consider the quantities $\Delta\rho$, etc. to be of a (uncorrelated) statistical nature with variances σ_ρ^2, etc. Equations (A23) then may be used to obtain equations for the standard deviations of the quantities $(\bar{S}^2+\bar{P}^2)$ and $\bar{T}^2$. Since the experimental results are in good agreement with the $V-A$ predictions we take the most probable values of $\Delta\rho$, etc. [and hence the most probable values for $(\bar{S}^2+\bar{P}^2)$ and $\bar{T}^2$] to be zero. Thus one writes

$$(\bar{S}^2+\bar{P}^2)\leq(8/3)g^2[\tfrac{9}{16}\sigma_h^2+36\sigma_\rho^2+\tfrac{9}{16}\sigma_\xi^2+(16/9)\sigma_\delta^2]^{1/2},$$

and (A24)

$$\bar{T}^2\leq\tfrac{4}{3}g^2[\tfrac{9}{16}\sigma_h^2+4\sigma_\rho^2+\tfrac{9}{16}\sigma_\xi^2+(16/9)\sigma_\delta^2]^{1/2}.$$

These inequalities are not invalidated by dropping the term $(V_+^2+A_+^2)$ which by definition satisfies $(V_+^2+A_+^2)\geq 0$. They have, over those given by Jarlskog, the advantage of being explicit upper bounds for the quantities of interest in terms of the errors in ρ, ξ, δ, and h. The upper bounds found by Jarlskog are more conservative (higher) than those found here because she, by using numerical methods, considered $(\bar{S}^2+\bar{P}^2)$ are $\bar{T}^2$ separately.

The most accurate values of the decay parameters and their weighted averages are given in Table VI. Using the data quoted in Table VI and assuming $|\hat{C}_S|=|\hat{C}_S'|$ $=|\hat{C}_P|=|\hat{C}_P'|$ and $|\hat{C}_T|=|\hat{C}_T'|$, one obtains

$$|\hat{C}_S|\leq 0.3g$$

and

$$|\hat{C}_T|\leq 0.3g,$$

where the entire limit[24] is due essentially to the error in helicity. These limits are identical for the coupling constants of the CR ordering, i.e., $|C_S|\leq 0.3g$, $|C_T|\leq 0.3g$; they could also be transformed into relationships for the $\tilde{C}_i$, but this is not done here because the relationships are rather cumbersome and involve the unknown $\hat{\epsilon}$ which would obscure their meaning.

TABLE VI. Experimental values for μ-decay parameters.

Parameter	Value	Reference
ρ[a]	0.780±0.025	Plano[g]
ρ[b]	0.750±0.003	Peoples[h]
ρ[b]	0.760±0.009	Sherwood[i]
ρ[b]	0.762±0.008	This experiment
ρ	0.756±0.006[f]	Weighted average
δ	0.78 ±0.05	Plano[g]
δ	0.782±0.031	Kruger[j]
δ	0.752±0.009	This experiment
δ	0.754±0.0085	Weighted average
ξ	0.97 ±0.05	Bardon *et al.*[k]
ξ	0.94 ±0.07	Plano[g]
ξ	0.975±0.015	Gurevich *et al.*[l]
ξ	0.973±0.014	Weighted average
h[c]	1.05 ±0.3	Buhler *et al.*[m]
h[c]	0.94 ±0.38	Bloom *et al.*[n]
h[c]	1.04 ±0.18	Duclos *et al.*[o]
h	−0.89 ±0.28	Schwartz[p]
h	(−)1.00 ±0.28	Weighted average
η[d]	−2.0 ±0.9	Plano[g]
η[e]	0.05 ±0.5	Peoples[h]
η[e]	−0.7 ±0.6	Sherwood[i]
η[e]	−0.7 ±0.5	This experiment

[a] One-parameter fit with an allowance in the error for $|\eta|\leq 0.44$.
[b] One-parameter fit, $\eta\equiv 0$.
[c] This experiment was done with positrons.
[d] Two parameter fit.
[e] One-parameter fit, $\rho\equiv\frac{3}{4}$.
[f] The error on ρ has been increased to allow for relaxation of the constraint $\eta\equiv 0$ to $|\eta|\leq 0.5$. This latter constraint is imposed both by the relationship $|\eta|<(1-h^2)^{1/2}$ and by the fact that $\rho\simeq\frac{3}{4}$. The author is indebted to Professor L. Michel for pointing out to him this constraint on η by the value of ρ. L. Michel, thesis, University of Paris, 1953 (unpublished).
[g] See Ref. 11.
[h] See Ref. 9.
[i] See Ref. 8.
[j] See Ref. 12.
[k] M. Bardon, D. Berley, and L. M. Lederman, Phys. Rev. Letters **2**, 56 (1959).
[l] See Ref. 26.
[m] A. Buhler, N. Cabbibo, M. Fidecaro, T. Massam, Th. Muller, M. Schneegans, and A. Zichichi, Phys. Letters **7**, 368 (1963).
[n] S. Bloom, L. A. Dick, L. Feuvrais, G. R. Henry, P. C. Macq, and M. Spighel, Phys. Letters **8**, 87 (1964).
[o] J. Duclos, I. Heintze, A. de Rujula, and V. Soergel, Phys. Letters **9**, 62 (1964).
[p] D. M. Schwartz, Phys. Rev. **162**, 1306 (1967).

APPENDIX B: FOURIER ANALYSIS OF THE PRECESSION CURVES

After the decay correction, it is assumed that the datum point N_{ij} is of the form

$$N_{ij}=M_i'\int_{\theta_j-\Delta\theta/2}^{\theta_j+\Delta\theta/2}[1+A_i\cos(\theta-\phi_i)]d\theta, \quad \text{(B1)}$$

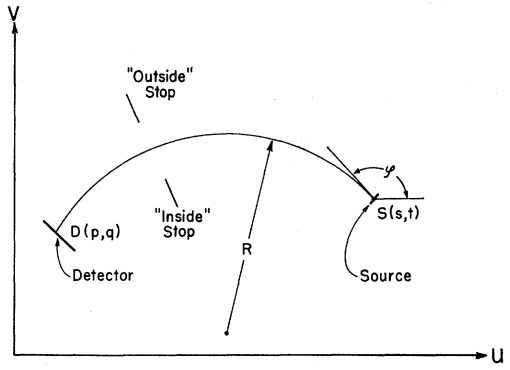

FIG. 9. Projection of the source (target) and the detector (final counter) onto the horizontal (u,v) plane. The magnetic field is vertical and into the paper. The (horizontal, vertical) coordinates of the source point S in the plane of the source are (s,t). The analogous coordinates of D are (p,q). The projection of an orbit passing through the points S and D between the occulting stops is shown. At S this orbit makes an azimuthal angle φ with the u axis.

where i and j are momentum and time indices, respectively, the prime indicates the inclusion of Ω, $\theta=\omega t$ is the muon precession angle, ϕ_i is the precession phase shift, and $\Delta\theta$ is the amount of precession included in one time bin (about 10 nsec). It is evident that the asymmetry A_i is proportional to the amplitude of the properly phased fundamental term in the Fourier decomposition of the ith set of N_{ij}. Specifically,

$$A_i=\frac{2\zeta}{N_i}\sum_{j=1}^{k}N_{ij}\cos(\omega t_j-\phi_i)\,, \tag{B2}$$

where

$$\zeta\equiv\frac{(\Delta\theta/2)}{\sin(\Delta\theta/2)}\,,\quad N_i\equiv\sum_{j=1}^{k}N_{ij}\,,$$

and k is the number of bins per precession cycle $(=2\pi/\Delta\theta)$. The factor ζ arises because the time bins are rectangular and of finite size. The variance of A_i is given by

$$\sigma^2(A_i)=(2\zeta^2/N_i)(1-\tfrac{1}{2}A_i^2)\,. \tag{B3}$$

APPENDIX C: SPECTROMETER SOLID ANGLE

The effective solid angle of the spectrometer, $\Omega(x)$, allowing for the finite size of the source, is given by

$$\Omega(x)=\int\Omega(x;s,t)W(s,t)dsdt\,, \tag{C1}$$

where $\Omega(x;s,t)$ is the geometric solid angle associated with a source point S at (s,t), W is a weighting factor proportional to the muon stop rate at S, and $dsdt$ is an element of source area. W is normalized by requiring that $\int Wdsdt=1$. See Fig. 9 for geometry.

We derive $\Omega(x;s,t)$ first. Consider a (rectangular) element of detector surface ΔA_{ij} at D (coordinates: p,q) where i and j are horizontal and vertical indices, respectively. ΔA_{ij} subtends $\Delta\Omega_{ij}(x;s,t)$ at S, and is chosen small enough so that $\Delta\Omega_{ij}(x,s,t)=\Delta\theta_j(x;s,t)\Delta\psi_i(x;s,t)$, where $\Delta\theta_j$ and $\Delta\psi_i$ are the mean vertical and horizontal apex angles of the (curved) pyramid which contains all (helical) trajectories of momentum x emanating from S and hitting ΔA_{ij}. The radius R and pitch angle θ of the helix satisfy

$$R=Kx\cos\theta \tag{C2}$$

and

$$\cos\theta=\frac{q-t}{2R\ \text{arc}\sin(d/2R)}\,, \tag{C3}$$

where d is the distance between S and D in the (u,v) plane and K is a constant. This pair of transcendental equations is conveniently solved for R and θ numerically. It is evident that

$$\Delta\theta=\frac{\Delta q\cos^2\theta}{2R\ \text{arc}\sin(d/2R)} \tag{C4}$$

and

$$\Delta\psi=\Delta\varphi\cos\theta\,, \tag{C5}$$

where Δq is the height of ΔA_{ij} and $\Delta\varphi$ is the angle subtended at S by the trace of ΔA_{ij} in the (u,v) plane. Simple geometrical arguments show that

$$\varphi=\pi+\text{arc}\tan\frac{v_S-v_D}{u_S-u_D}-\text{arc}\sin(d/2R)\,; \tag{C6}$$

$\Delta\varphi$ is obtained by numerical differentiation.

In order to allow for possible occultation of the detector by the edges of the chambers (the relevant chambers are R3 and P2) a source-point weight factor $\gamma_{ij}(x;s,t)$ is assigned to each $\Delta\Omega_{ij}(x)$. The trajectories of smaller radii are occulted by the outside stop while those of larger radii by the inside stop. γ varies from 0 to 1 according to the fraction of ΔA_{ij} which is illuminated from S by particles of momentum x. Thus, one writes

$$\Omega(x;s,t)=\sum_{i,j}\gamma_{ij}(x;s,t)\Delta\Omega_{ij}(x;s,t)\,. \tag{C7}$$

To determine the detail necessary to describe $W(s,t)$, we examine the change in "shape" of $\Omega(x;s,t)$ as S moves within the source. Using the mean relative slope $\langle\partial\ln\Omega/\partial x\rangle$ as a quantitative index of shape, we compute $\langle\partial^2\ln\Omega/\partial t\partial x\rangle=0.0004$/in. and $\langle\partial^2\ln\Omega/\partial s\partial x\rangle=0.34$/in. for vertical[31] and horizontal displacements, respectively. Expressed in terms of fits for ρ, these source-point motions lead, through Ω, to $\partial\rho/\partial t\cong-10^{-4}$/in. and $\partial\rho/\partial s=-0.13$ in. It is clear from these numbers that vertical variations in W may be neglected, but horizontal variations of W must be considered. Physically, the negligible dependence of Ω

[31] The values quoted for $\partial^2\ln\Omega/\partial t\partial x$ and $\partial\rho/\partial t$, are actually rms values since by symmetry the mean values must vanish.

upon t is reasonable because the pitch angle, θ, is quite small in this spectrometer; the large dependence upon s is a result of the occultation effect.

The source brightness B (observed density of muon decays per unit source area) is obtainable from the data since the trajectory of each event is known, and B, in fact, is already a very good approximation to W. That B is not identical to W is due to the fact that $\Omega(x;s,t)$ is somewhat larger for source points nearer the detector; these points appear brighter on an illumination plot normalized to the local muon stop rates. B was obtained by observing events in the range $0.43 \leq x \leq 0.57$, for which $\gamma = 1$. This range contains about one-half of the total events. Using this B, the source was then divided into three equally bright vertical strips, and the centroids of these strips were found. These centroids were then subjected to a 0.02-in. horizontal displacement (toward the outside of the source) to account for the fact that $(1/\Omega)\partial\Omega/\partial s = -0.043$/in. in the above momentum range. The correction to ρ to account for neglecting the shape of the stops distribution in the vertical is estimated to be $\Delta\rho = -0.0002$. The correction needed because three instead of an infinite number of strips were used is estimated to be 0.0004.

A plot of $\Omega(x)$ is given in Fig. 5.

PHYSICAL REVIEW VOLUME 166, NUMBER 5 25 FEBRUARY 1968

Search for Fractionally Charged Particles*

E. H. BELLAMY,† R. HOFSTADTER, AND W. L. LAKIN
High Energy Physics Laboratory, Stanford University, Stanford, California

AND

M. L. PERL AND W. T. TONER
Stanford Linear Accelerator Center, Stanford University, Stanford, California

(Received 16 October 1967)

A search was made for fractionally charged particles produced by 12-GeV electrons incident on a copper target. No such particles were detected. Comparison with calculations on photoproduction of pairs of these particles enable lower limits to be placed on the masses of such particles if they exist. Particles of the type discussed in this paper (pure spin-$\frac{1}{2}$ Dirac particles with no strong interactions) do not exist with masses below these limits. These limits are dependent on the charge and lifetime assigned to the particle. For lifetimes $\geq 10^{-7}$ sec, the lower limit varies from 0.2 GeV for $0.04e$ charge, to 1.5 GeV for $0.7e$ charge. For lifetimes $\geq 10^{-8}$ sec and $0.7e$ charge, the lower limit is 1.1 GeV.

INTRODUCTION

THERE have been a number of experiments[1–8] designed to detect fractionally charged particles since the idea of quarks was introduced by Gell-Mann[9] and Zweig.[10] Experiments at proton accelerators have failed to find quarks with production ratios, compared to pions of the same momenta of $\sim 5\times 10^{-9}$ for charge $e/3$, and $\sim 4\times 10^{-8}$ for charge $2e/3$. Cosmic-ray experiments place limits of $\sim 10^{-8}$ of the muon flux for charge $e/3$ or $2e/3$ particles. Foss *et al.*[8] have searched for fractionally charged particles with charges from $e/3$ to $2e/3$ using the Cambridge electron accelerator. This experiment, which was similar in concept to ours, used a 6.0-GeV bremsstrahlung beam incident on a carbon target. They found no fractionally charged particles. Using the Bethe-Heitler pair production cross section they were able to show that no particles exist with

$$[\text{charge } e/3] \text{ and } [0.5 \text{ MeV} \leq \text{mass} \leq 780 \text{ MeV}],$$
$$[\text{charge } 2e/3] \text{ and } [2.0 \text{ MeV} \leq \text{mass} \leq 840 \text{ MeV}].$$

These limits are for non-strongly-interacting particles with relatively long lifetimes.

The high-energy, high-intensity electron beam at the Stanford linear accelerator center offers the opportunity

* Work supported in part by the U. S. Office of Naval Research, Contract [Nonr 225(67)] and by the Atomic Energy Commission. Distribution of this document is unlimited.

† On leave of absence from Westfield College, University of London, England.

[1] D. R. O. Morrison, Phys. Letters **9**, 199 (1964).

[2] H. H. Bingham, M. Dickinson, R. Diebold, W. Koch, D. W. G. Leith, M. Nikolić, B. Ronne, R. Huson, P. Musset, and J. J. Veillet, Phys. Letters **9**, 201 (1964).

[3] V. Hagopian, W. Selove, R. Ehrlich, E. Leboy, R. Lanza, D. Rahm, and M. Webster, Phys. Rev. Letters **13**, 280 (1964).

[4] W. Blum, S. Brandt, V. T. Cocconi, O. Czyzewski, J. Danysz, M. Jobes, G. Kellner, D. Miller, D. R. O. Morrison, W. Neale, and J. G. Rushbrooke, Phys. Rev. Letters **13**, 353a (1964).

[5] P. Franzini, B. Leontic, D. Rahm, N. Samios, and M. Schwartz, Phys. Rev. Letters **14**, 196 (1965).

[6] R. C. Lamb, R. A. Lundy, T. B. Novey, and D. D. Yovanovitch, Phys. Rev. Letters **17**, 1068 (1966).

[7] H. Kasha, L. B. Leipuner, and R. K. Adair, Phys. Rev. **150**, 1140 (1966).

[8] J. Foss, D. Garelick, S. Homma, W. Lobar, L. S. Osborne, and J. Uglum, Phys. Letters **25B**; 166 (1967); G. Bathow *et al.*, *ibid.* **25B**, 163 (1967).

[9] M. Gell-Mann, Phys. Letters **8**, 214 (1964).

[10] G. Zweig, CERN Report No. 8182/TH 401, 1964 (unpublished).